Transverse Isotropic Behavior Identification using Digital Image Correlation of a Pre-structured Material Manufactured by 3D Printing

Marouene Zouaoui, Julien Gardan, Pascal Lafon, Carl Labergere, Ali Makke, Naman Recho

Available online at www.sciencedirect.com

ScienceDirect

Structural Integrity Procedia 00 (2019) 000–000

Structural Integrity Procedia

www.elsevier.com/locate/procedia

1st Virtual European Conference on Fracture

Transverse Isotropic Behavior Identification using Digital Image Correlation of a Pre-structured Material Manufactured by 3D Printing

Marouene Zouaoui*[1,2], Julien Gardan[1,2], Pascal Lafon[1], Carl Labergere[1], Ali Makke[2], Naman Recho[2,3]

1 Institut Charles Delaunay, LASMIS, UTT,UMR CNRS 6281, 12 rue Marie Curie, 10010 Troyes, France
2 EPF, Engineering school, 2 rue Fernand Sastre, Troyes, France
3 Pascal Institute, Blaise Pascal University, 63000 Clermont Ferrand, France

Abstract

This work aims to develop an advanced structured material [1] that enhances the physical properties in the fracture mechanics area with specimens printed by FDM. 3D printed parts are considered as complex structures and assumed to show a strong anisotropy related to deposition trajectories, air gaps, and welding lines. Therefore, a challenging problem that arises in this domain is the difficulty of predicting the mechanical behavior and controlling the physic properties of parts (tensile strength and fracture toughness…).

An extrusion deposition method was proposed involving the use of a controlled deposition method to improve the fracture toughness of FDM parts [2], [3].The enhancement is based on a filament deposition optimization in order to reproduce principal stresses directions in a region of interest submitted to crack initiation around the notch tip.

The overall goal of this research is to identify material constants from experimental tests. Those constants will be used then as inputs of a finite element model, which tackles to include the structural anisotropy by assigning materials references into local mesh elements [4]. Thus, the corresponding behavior was assumed to be transverse isotropic and five elastic materials constants must be identified. Hence, a set of tensile tests was performed with full-field measurements by Digital Image Correlation (DIC) for different filament orientations. Regions of interests were chosen according to the local loading state to activate specific materials constants. The experiments outcomes prove that 3D printed specimens have unexpectedly isotropic stiffness due to similar values found of longitudinal and

* Corresponding author. Tel.: +33 (0)3 25 71 76 00.
E-mail address: marouene.zouaoui@utt.fr

transversal Young's modulus 1680 MPa and 1414 MPa respectively. Although anisotropy is well highlighted when we consider tensile strength. On the light of these results, the model will be enriched by implementing a Hill yield criterion to better represent the observed plastic anisotropic behavior.

The main contribution is to validate the numerical model inputs that reproduce the measured experimental fields, and later on develop an identification based on an Updated Finite Element Model Updated (UFEM).

Keywords: Fused Deposition modeling, Fracture Mechanics, Additive Manufacturing, Transverse isotropic behavior, FEM, Local references orientations

1. Introduction

Most of the sectors are developing the industry of the future or 4.0 with strong expectations for Additive Manufacturing. Advanced applications, such as aeronautics and automotive, which required the implementation of complex assemblies of several components present a major challenge for manufacturers. The integration of functional or "smart" materials is considered at this level as an optimal solution to answer to a number of needs. A smart material is defined according to Gardan et al [1] as a static or a dynamic reaction of complex shapes with a material's combination to achieve one or more properties in order to respond to a predefined functionality. The importance of additive manufacturing is therefore highlighted since it makes it possible to produce more optimized structures and more complex shapes than with conventional manufacturing processes. Thus, it allows the development of advanced materials. This work is part of a study that deals with developing pre-structured materials using Fused Deposition Modeling (FDM) process and studying their mechanical behavior. Its main purpose is to identify the elastic constants of a pre-structured material fabricated based on a fracture toughness strengthening where the filaments are oriented according to principal stress directions. Improvement of fracture toughness of both CT specimen [2] and bending Beam specimen [5] stands proof of this method's efficiency. The major goal is to establish a numerical model that predict with a high accuracy the fracture behavior of this pre-structured material.

Table 1. The elastic constants for the transversely isotropic material

Elastic constant	designation
Longitudinal Young's modulus	$\boldsymbol{E_L}$
Transverse Young's modulus	$\boldsymbol{E_T}$
In plane Poisson's ratio	$\boldsymbol{\nu_{LT}}$
In plane shear modulus	$\boldsymbol{G_{LT}}$
Out of plane Poisson's ratio	$\boldsymbol{\nu_{TT}}$

2. Transverse isotropic behavior for 3D printed material

Due to filaments orientations and the built procedure, 3D printed materials are assumed to have an anisotropic behavior. To study their behavior an orthotropic law is commonly used. Zhao and al. developed a mechanical model that highlights the anisotropic tensile strength and elastic property of PLA material supposing an orthotropic behavior [6]. While Alaimo and al. utilized the Classical Lamination Theory (CLT) and Tsai-Hill yielding criterion to predict in-plane stiffness and strength of FDM specimens[7].Likewise Dai and al. identified orthotropic elastic constants of PLA material using an experimental investigation [8]. Furthermore, a transversely isotropic model is put forward in form of constitutive equations and is compared with an isotropic model considering the influence of printing orientation to model the mechanical behavior of 3D printed ABS material [9].

If we compare the transverse direction in the built plane and the built direction, we can clearly observe a built similarity. A transverse isotropic behavior is therefore chosen. Such material has five independent elastic constants. Table 1 presents the designation that will be used for this study.

3. Experimental identification of material's elastic constants

3.1. 3D printing

Tensile specimens were designed according to ASTM D638-03, "Standard Test Method for Tensile Properties of Plastics" [10]. White ABS (Acrylonitrile Butadiene Styrene) filament was used for the purpose of having a better contrast while applying the black speckle. All specimens were printed on A Makerbot replicator x2 in a flat configuration using a layer thickness of 0.25 mm. The filament was extruded at 235°C on a preheated built plate at 120°C. Each specimen was made of 28 Layer. For the infill angle, three kinds of specimen were printed .longitudinal (L) and transverse (T) and 45° directions. The modifier feature of the slicing software Slic3r [11] was used to get a unique infill angle for all layers.

3.2. Tensile test with Digital Image correlation

The tensile tests were performed on a tensile test machine Instron 4411. A loading rate of 1 mm/min was used. In order the get accurate results using the DIC method one snapshot was saved every 0.6 s during the test. For every tensile test, three Regions Of Interest (ROI) were selected as shown in figure 1.

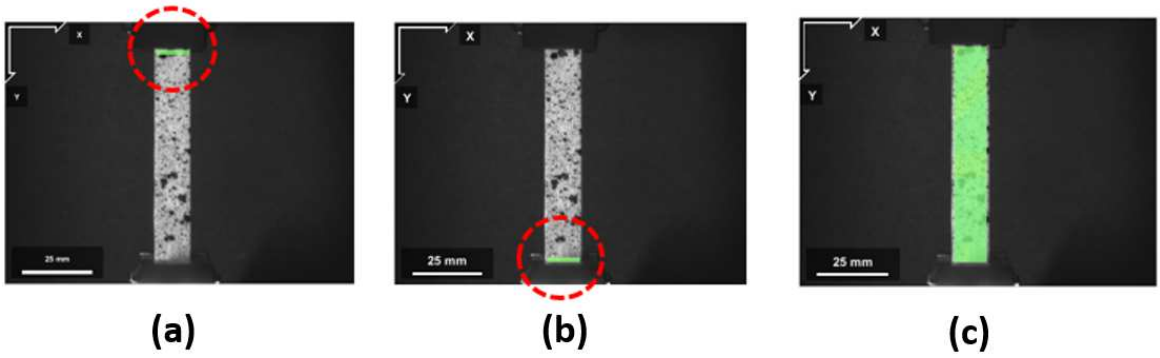

Fig. 1. Regions of interest definition: (a) Upper ROI; (b) Lower ROI; (c) Total ROI

While performing the tests numerous problems occur, mainly slip problems and filaments delamination between the jaws. For such reason a method was used to access the true value displacement value of the specimen. It can be calculated as the difference between the average displacements calculated over the Upper ROI and the Lower ROI. The total ROI used to calculate the Poisson's ratio. The mean values of both longitudinal and transversal strains are calculated in a range between a starting snapshot and the snapshot 200 (approximately the elastic region for all specimens). The negative value of the transversal strain is plotted as a function of the longitudinal one. The slope gives the value of the Poisson's ratio. This ROI will be later on used for the numerical model validation while comparing measured experimental and numerical strain fields.

3.3. Identified elastic constants

For the experimental identifications, three elastic constants are directly calculated through the tensile tests (Longitudinal and transverse Young's modulus ($\boldsymbol{E_L}$, $\boldsymbol{E_T}$) and the in plane Poisson's ratio $\boldsymbol{\nu_{LT}}$). The in plane shear modulus $\boldsymbol{G_{LT}}$ is calculated through the stress analysis of the 45° specimen. Using the stress analysis of fibre reinforced composite material's [12] a relation (see equation 1) between the shear modulus and the calculated Young's modulus and Poisson's ratio is established.

$$\boldsymbol{G_{LT}} = \left(\frac{\mathbf{4}}{\boldsymbol{E_{45°}}} - \frac{\mathbf{1}}{\boldsymbol{E_L}} - \frac{\mathbf{1}}{\boldsymbol{E_T}}\right.$$

Where:

- $\boldsymbol{E_L}$: Young's modulus in the longitudinal direction
- $\boldsymbol{E_T}$: Young's modulus in the transverse direction
- $\boldsymbol{\nu_{LT}}$: In plan Poisson's ratio
- $\boldsymbol{E_{45°}}$: Experimental Young's modulus of the 45° specimen

The out of plane Poisson's ratio ($\boldsymbol{\nu_{TT}}$ **:** in the isotropy plane) cannot be identified using the available data. Here plane stress loadings are studied and $\boldsymbol{\nu_{TT}}$ has no influence on the in plane material behavior. Since it only affects the out of plane strain component. By analyzing the compliance matrix components for the transversely isotropic material $\boldsymbol{\nu_{TT}}$ is only activated when off plane shear loading is applied or by measuring the out of plane displacement. Therefore , for the numerical model, an average value between the Poisson's ratios calculated using the transverse specimen $\boldsymbol{\nu_{TL}}$ and the longitudinal specimen $\boldsymbol{\nu_{LT}}$ is used.

It is important to consider the air gap (voids inside a 3D printed part) while calculating the Young's modulus since it influences directly the mechanical behavior of the material. Otherwise, getting an accurate estimation of the air gap is difficult. Therefore, in order to avoid such calculation that possibly adds another source of error and especially to keep the global dimensions of the part while creating the numerical model, the engineering stress was calculated using the effective measured section of the specimen.

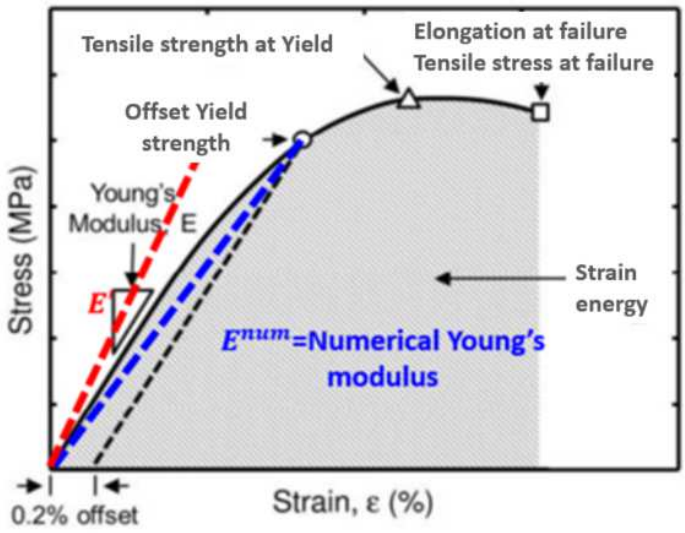

Fig. 2. Young's modulus calculation method; Red line: slope of the tangent method; Blue line: linear elastic behavior assumption

As previously announced, this work is part of developing a full numerical model of the pre-structured material that goes until fracture. Thus reaching the yielding point with the right stress and the right strain levels is crucial. Since an elastic non-linearity was observed, calculating Young's modulus as the slope of the tangent to the true stress-strain curve at low stress will lead to an under estimations of the strain at the yielding point. This is why another method for calculating Young's modulus was used. It consists of considering a linear elastic behavior until the yielding point calculated with an offset of 0.2 % strain.

4. Finite element model validation

In order to check the validity of the identified elastic constants, an oriented numerical model for each specimen will be created. The local references in mesh element assignment method described in [4] will be used to reproduce the printing orientation inside the model. The numerical answer will be compared to collect data using the DIC analysis.

The cost function was formulated based on the Finite Element Model Updated widely used [13]–[15] that represents an inverse method to identify the inputs of a numerical model. The validity of those inputs is related to their capacity the reproduce experimental results (fields measurement) with a low level of error. The objective here is to evaluate the difference between the numerical and experimental forces as well as the difference between the DIC and numerical strain fields while using the identified material's constants ($\boldsymbol{E_L}$, $\boldsymbol{E_T}$, $\boldsymbol{\nu_{LT}}$, $\boldsymbol{G_{LT}}$) ,except $\boldsymbol{\nu_{TT}}$ that was proved to have no influence on the formulated cost function.

4.1. Subsets and Integration points linking

A linking procedure was performed between the subsets of the reference snapshot and the integration points of the undeformed mesh. The density of subsets is higher than the integration points, so it was decided to reduce the experimental data size to fit the number of integration points by linking each one to the neighbor subsets within a radius less than half the used mesh seize. The following figure shows the reference snapshot localized on the undeformed finite element mesh of the tensile specimen.

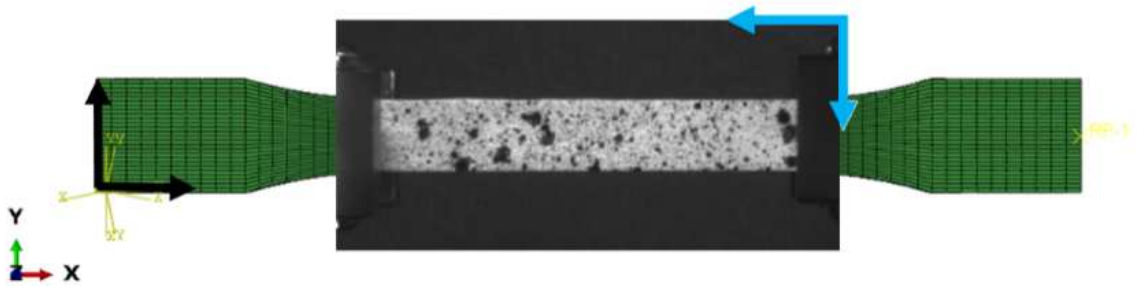

Fig. 3. Reference snapshot linked with the undeformed mesh

4.2. Loading steps choice

Several loading steps were chosen from the start of the test until the yielding point. Such choice was mad to ensure the prediction accuracy of the mechanical behavior of the pre-structured material. After computing the cost function for each loading step it was decided to discard the steps at low levels of strain and load. Such choice was made knowing that low strain values are easily perturbed by the noise and the measured load values are affected by the loading phase (slip between the jaws).

4.3. Cost function formulation

The equation 2 represents the full cost function that can be divided into two components. A cost function for the strain fields comparison and the other one for the force comparison.

$$\boldsymbol{e_{i\{1\dots M\}.avg.full}} = \frac{\mathbf{1}}{\mathbf{2NM}}\sum_{\boldsymbol{i}}^{\boldsymbol{M}}\sum_{\boldsymbol{n}}^{\boldsymbol{N}}\left(\frac{\left\|\boldsymbol{\varepsilon}_{\boldsymbol{i.n}}^{\boldsymbol{ABAQUS}} - \boldsymbol{\varepsilon}_{\boldsymbol{i.avg\{p_1\dots p_l\}}}^{\boldsymbol{DIC}}\right\|}{\left\|\boldsymbol{\varepsilon}_{\boldsymbol{i.avg\{p_1\dots p_l\}}}^{\boldsymbol{DIC}}\right\|}\right) + \frac{\mathbf{1}}{\mathbf{2M}}\sum_{\boldsymbol{i}}^{\boldsymbol{M}}\left(\frac{\left\|\boldsymbol{F}_{\boldsymbol{i}}^{\boldsymbol{ABAQUS}} - \boldsymbol{F}_{\boldsymbol{i}}^{\boldsymbol{DIC}}\right\|}{\left\|\boldsymbol{F}_{\boldsymbol{i}}^{\boldsymbol{DIC}}\right\|}\right) \quad (2)$$

The experimental strain field $\varepsilon_{i.s}^{DIC}$ calculated for the snapshot i and overall the subsets s on the ROI will be compared with the numerical strain field $\varepsilon_{i.n}^{ABAQUS}$ calculated for the simulation i (or snapshot i) over all the integration points n inside the ROI. As said before a procedure was performed in order to link every integration point n with the neighbor subsets$\{p_1 \dots p_l\}$ where an average value will be used for comparison. N presents the number of integration points inside the ROI. In addition, the numerical force F_i^{ABAQUS} is compared to the experimental one F_i^{DIC}. The final cost function is a computation of this comparison over the M chosen loading steps. For the strain field comparison only two components were used (the longitudinal and the transverse strains).

5. Results and discussions

5.1. Experimental results

Table 2 presents the founding of the experimental identification compared to data collected from the literature. For comparison, an equivalent printing configuration is mandatory (flat configuration, layer thickness, temperature, used filament, etc…). Young's modulus as announced before was calculated via two methods. Results are coherent with the literature despite the differences in the elastic modulus, which can be related to some different parameters while printing the specimen or the used type of ABS filament.

Table 2. Results of the experimental identification

Elastic constant	slope of the tangent method	linear elastic behavior assumption	Rodríguez and al. 2001 [16]	Alaimo and al. 2017 [7]
E_L (MPa)	1680 ± 71	1476	1921.6 ± 17	2010 ± 153
E_T (MPa)	1414 ± 133	1309	1621± 24	1671 ± 57
ν_{LT}	0.3710 ± 0.032	0.3710 ± 0.032	0.37 ± 0.014	0.32 ± 0,1
G_{LT} (MPa)	545	478	672.5	641 ± 47
ν_{TT}	-	-	-	-

Unforeseen, the material seems to have an overall isotropic behavior because Young's modulus has a slight difference between each other. This means that welding lines are not affecting the material stiffness and the anisotropy was mainly observed at the yielding stress and the tensile strength.

For the isotropy plane Poisson's ratio, an experimental protocol is under development allowing us to measure the out of plane displacement and then identify its value.

5.2. Cost function evaluation

For the numerical model, a value $\boldsymbol{\nu_{TT}}$ =0.3416 will be used. The results are shown below (Table 3). Both used elastic sets of constants independently from the calculation method are giving an accurate estimation of strain fields. This proves that the model can predict transversally strain using the identified Poisson's ratio. High levels of error

for the load cost function are explained by the non-linearity observed with the true tensile curves. By comparing the full cost functions, it is clear that the linear approach is more adequate to our study. Especially, knowing that the major goal of the project is to go later on until fracture.

Table 3. Cost function calculation

Input calculation method	slope of the tangent method			linear elastic behavior assumption		
Cost function (%)	$e_{i\{1\dots M\}.load}$	$e_{i\{1\dots M\}.strain}$	$e_{i\{1\dots M\}.avg.full}$	$e_{i\{1\dots M\}.load}$	$e_{i\{1\dots M\}.strain}$	$e_{i\{1\dots M\}.avg.full}$
L	11.34	5.78	8.61	5.51	5.43	4.47
T	15.90	11.71	13.81	8.76	8.83	8.80
45°	15.88	4.73	10.30	9.12	4.07	6.59

5.3. Beam A specimen

The experimental results issued from reference [5] will be utilized to check the validity of the previously identified elastic constants. Beam A geometry defined by Li and al. [17] was printed using two different deposition methods, a classical specimen with ± 45° orientation and an optimized specimen where the reinforcement method is applied.

As the graph presented in figure 4 both numerical models are giving similar predictions of the load although the optimized specimens are stiffer than the classical ones. The model is not yet able to highlight the difference of stiffness that could be explained because of the almost isotropic elastic behavior and a layer-by-layer orthogonally building process.

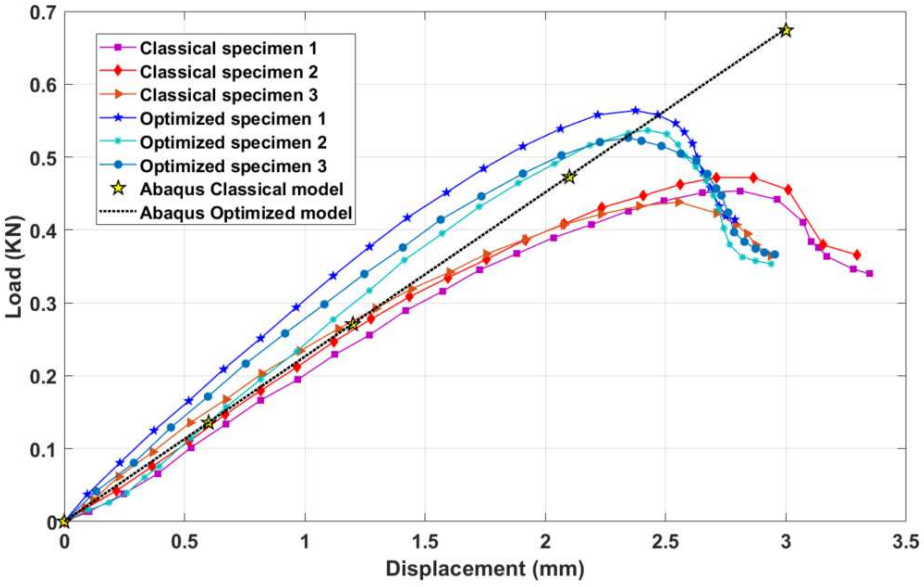

Fig. 4. Numerical model response compared to experimental bending tests; Classical specimen printed with ± 45° infill and optimized specimen printed using the reinforcement method

6. Conclusion

The mechanical behavior of the pre-structured material fabricated by FDM process was studied in the elastic domain. It was observed that stiffness wise the material has a globally isotropic behavior since both Young's modulus are slightly different. Another founding concerns the global answer of Beam A specimen that remained the same even with the optimized deposition method. This is directly related to the previous result announcing the elastic behavior as isotropic. Moreover, in such geometry the number of layers is very high with a layer alternation strategy where filaments are orthogonally deposited. On the other hand, the anisotropy was well highlighted while comparing the yielding points and the fracture stress. Therefore, a Hill criterion will be used to model this aspect.

The developed procedure of comparison using the formulated cost function can also be used to identify all four accessible elastic constants through an inverse method. The research orientation is to minimize the error between the experimental data and the numerical over pre-selected ROI where the local loading stress on the filaments is known.

Acknowledgements

The authors gratefully acknowledge the Grand-Est region in France and the European Regional Development Fund (ERDF), University of Technology of Troyes and EPF Engineering School of Troyes for their financial support.

References

[1] J. Gardan, 'Smart materials in additive manufacturing: state of the art and trends', *Virtual and Physical Prototyping*, vol. 14, no. 1, pp. 1–18, Jan. 2019, doi: 10.1080/17452759.2018.1518016.

[2] J. Gardan, A. Makke, and N. Recho, 'Improving the fracture toughness of 3D printed thermoplastic polymers by fused deposition modeling', *International Journal of Fracture*, vol. 210, no. 1–2, pp. 1–15, Mar. 2018, doi: 10.1007/s10704-017-0257-4.

[3] J. Gardan, A. Makke, and N. Recho, 'A Method to Improve the Fracture Toughness Using 3D Printing by Extrusion Deposition', *Procedia Structural Integrity*, vol. 2, pp. 144–151, 2016, doi: 10.1016/j.prostr.2016.06.019.

[4] M. Zouaoui *et al.*, 'Numerical Prediction of 3D Printed Specimens Based on a Strengthening Method of Fracture Toughness', *Procedia CIRP*, vol. 81, pp. 40–44, 2019, doi: 10.1016/j.procir.2019.03.008.

[5] P. Lanzillotti, J. Gardan, A. Makke, and N. Recho, 'Enhancement of fracture toughness under mixed mode loading of ABS specimens produced by 3D printing', *RPJ*, vol. 25, no. 4, pp. 679–689, May 2019, doi: 10.1108/RPJ-09-2018-0247.

[6] Y. Zhao, Y. Chen, and Y. Zhou, 'Novel mechanical models of tensile strength and elastic property of FDM AM PLA materials: Experimental and theoretical analyses', *Materials & Design*, vol. 181, p. 108089, Nov. 2019, doi: 10.1016/j.matdes.2019.108089.

[7] G. Alaimo, 'Influence of meso-structure and chemical composition on FDM 3D-printed parts', *Composites Part B*, p. 10, 2017.

[8] S. Dai, Z. C. Deng, Y. J. Yu, K. Zhang, S. H. Wang, and J. Ye, 'Orthotropic elastic behaviors and yield strength of fused deposition modeling materials: Theory and experiments', *Polymer Testing*, vol. 87, p. 106520, Jul. 2020, doi: 10.1016/j.polymertesting.2020.106520.

[9] R. Zou *et al.*, 'Isotropic and anisotropic elasticity and yielding of 3D printed material', *Composites Part B: Engineering*, vol. 99, pp. 506–513, Aug. 2016, doi: 10.1016/j.compositesb.2016.06.009.

[10] D20 Committee, 'Test Method for Tensile Properties of Plastics', ASTM International. doi: 10.1520/D0638-14.

[11] 'Slic3r Manual – Welcome to the Slic3r Manual'. https://manual.slic3r.org/ (accessed Jun. 24, 2020).

[12] M. W. Hyer, *Stress analysis of fiber-reinforced composite materials*, Updated edition. Lancaster, Pennsylvania: DEStech Publications, Inc, 2009.

[13] L. ROBERT, V. Velay, N. Decultot, and S. Ramde, 'Identification of hardening parameters using finite element models and full-field measurements: some case studies', *Journal of Strain Analysis for Engineering Design*, vol. 47, no. 1, pp. 3–17, Jan. 2012, doi: 10.1177/0309324711430022.

[14] J. Kajberg and G. Lindkvist, 'Characterisation of materials subjected to large strains by inverse modelling based on in-plane displacement fields', *International Journal of Solids and Structures*, vol. 41, no. 13, pp. 3439–3459, Jun. 2004, doi: 10.1016/j.ijsolstr.2004.02.021.

[15] P. Sztefek and R. Olsson, 'Tensile stiffness distribution in impacted composite laminates determined by an inverse method', *Composites Part A: Applied Science and Manufacturing*, vol. 39, no. 8, pp. 1282–1293, Aug. 2008, doi: 10.1016/j.compositesa.2007.10.005.

[16] J. F. Rodríguez, J. P. Thomas, and J. E. Renaud, 'Mechanical behavior of acrylonitrile butadiene styrene (ABS) fused deposition materials. Experimental investigation', *Rapid Prototyping Journal*, vol. 7, no. 3, pp. 148–158, Aug. 2001, doi: 10.1108/13552540110395547.

[17] J. Li, X.-B. Zhang, and N. Recho, 'J–Mp based criteria for bifurcation assessment of a crack in elastic–plastic materials under mixed mode I–II loading', *Engineering Fracture Mechanics*, vol. 71, no. 3, pp. 329–343, Feb. 2004, doi: 10.1016/S0013-7944(03)00117-6.